



Published in final edited form as:

*J Thorac Cardiovasc Surg.* 2022 February ; 163(2): e161–e171. doi:10.1016/j.jtcvs.2020.06.028.

## Novel Bicuspid Aortic Valve Model with Aortic Regurgitation for Hemodynamics Analysis Using an *Ex Vivo* Simulator

Yuanjia Zhu, MD<sup>1,2,\*</sup>, Annabel M. Imbrie-Moore, MS<sup>1,3,\*</sup>, Michael J. Paulsen, MD<sup>1</sup>, Bryant Priromprinr, MD<sup>4</sup>, Hanjay Wang, MD<sup>1</sup>, Haley J. Lucian, BA<sup>1</sup>, Justin M. Farry, BSE<sup>1</sup>, Y. Joseph Woo, MD<sup>1,2</sup>

<sup>1</sup>:Department of Cardiothoracic Surgery, Stanford University, Stanford, CA

<sup>2</sup>:Department of Bioengineering, Stanford University, Stanford, CA

<sup>3</sup>:Department of Mechanical Engineering, Stanford University, Stanford, CA

<sup>4</sup>:Department of Pediatrics, Division of Pediatric Cardiology, Stanford University, Stanford, CA

### Abstract

**Objective:** The objective was to design and evaluate a clinically relevant, novel *ex vivo* bicuspid aortic valve model that mimics the most common human phenotype with associated aortic regurgitation.

**Methods:** Three bovine aortic valves were mounted asymmetrically in a previously validated 3D-printed left heart simulator. The non-right commissure and the non-left commissure were both shifted slightly towards the left-right commissure, and the left and right coronary cusps were sewn together. The left-right commissure was then detached and re-implanted 10 mm lower than its native height. Free margin shortening was used for valve repair. Hemodynamics, high-speed videography, and echocardiography data were collected before and after the repair.

**Results:** The bicuspid aortic valve model was successfully produced and repaired. High-speed videography confirmed prolapse of the fused cusp of the baseline bicuspid aortic valve models in diastole. Hemodynamics and pressure data confirmed simulation of physiologic diseased conditions with aortic regurgitation and the subsequent success of repair. Regurgitant fraction post-repair was significantly reduced compared to that at baseline ( $28.6 \pm 3.4\%$  versus  $14.5 \pm 4.4\%$ ,  $p=.037$ ). There was no change in peak velocity, peak gradient, or mean gradient across the valve pre- vs. post-repair:  $292 \pm 18.3$  cm/s versus  $325.3 \pm 58.2$  cm/s ( $p=.29$ ),  $34.3 \pm 4.2$  mmHg versus  $43.3 \pm 15.4$  mmHg ( $p=.30$ ), and  $11 \pm 1$  mmHg versus  $9.3 \pm 2.5$  mmHg ( $p=.34$ ), respectively.

**Conclusions:** An *ex vivo* bicuspid aortic valve model was successfully designed and recapitulated the most common human phenotype with aortic regurgitation. These valves were

---

**Corresponding Author:** Y. Joseph Woo, MD, 300 Pasteur Drive, Falk Cardiovascular Research Center, Department of Cardiothoracic Surgery, Stanford University School of Medicine, Stanford, CA 94305, P:650-725-3828; F:650-725-3846, joswoo@stanford.edu.  
\*Co-first author

**Publisher's Disclaimer:** This is a PDF file of an unedited manuscript that has been accepted for publication. As a service to our customers we are providing this early version of the manuscript. The manuscript will undergo copyediting, typesetting, and review of the resulting proof before it is published in its final form. Please note that during the production process errors may be discovered which could affect the content, and all legal disclaimers that apply to the journal pertain.

**DISCLOSURES** None.

successfully repaired, confirming its potential for evaluating valve hemodynamics and optimizing surgical repair for bicuspid aortic valves.

## CENTRAL MESSAGE

A regurgitant bicuspid aortic valve model recapitulates the most common human phenotype, providing a key avenue for repair analysis.

---

## INTRODUCTION

Bicuspid aortic valve (BAV) is one of the most common congenital defects with an estimated prevalence of 0.5% to 2%<sup>1,2</sup>. The morphology of BAV varies depending on the cusp fusion pattern and the presence of raphe<sup>3</sup>. The left-right cusp fusion pattern is the most common phenotype, encompassing 71% of BAV leaflet patterns<sup>3</sup>. Typically, the surface area of the two leaflets are unequal, and the free edge of the fused cusp usually exceeds that of the nonfused cusp<sup>4</sup>. Additionally, as the commissural orientation is altered from a symmetrical to a non-symmetrical configuration, the fusion length decreases and the non-functional commissure height increases<sup>5</sup>. Both factors contribute to aortic regurgitation (AR) due to prolapse of the fused cusp. BAV repair primarily consists of correcting the prolapse of the fused cusp<sup>6-8</sup>. Some of the techniques frequently employed to repair BAV with AR include: raphe resection, leaflet plication, free margin shortening, and pledgeted commissuroplasty<sup>9-10</sup>. Valve-sparing root replacement has also been utilized recently to address AR due to annular dilation<sup>5-11</sup>. However, increased systolic gradients have been observed after BAV repairs<sup>11,12</sup>, and the repair durability of BAV is unclear.

*Ex vivo* heart simulators enable investigation of valvular biomechanics in a controlled environment. Previous studies have demonstrated their ability and advantage in evaluating various valvular dysfunctions, surgical repair techniques and surgical device innovation<sup>13-16</sup>. Although a number of aortic valve surgical repair techniques have been described and are currently being used clinically, there is a paucity of hemodynamic evaluation of these techniques<sup>6-8,10-12</sup>. Furthermore, a valid, clinically relevant BAV model that closely mimics the most common human BAV phenotype with AR is needed to investigate valvular hemodynamics before and after repair. In this study, we describe a novel BAV model with a left-right cusp fusion pattern and associated AR using explanted bovine aortic valve secured in a porcine-sized aortic mount. We subsequently examine the repair of our model to explore the efficacy of such a model to optimizing surgical techniques. The development of this model will enable us to perform thorough quantitative evaluation of the characteristics, hemodynamics and repair techniques for the most common phenotype of human BAV, thus having a significant potential impact on current clinical practice and providing an avenue for the development of new hemodynamically optimal surgical repair techniques.

## METHODS

### Model Design

Bovine hearts (n=3) explanted from cows weighing between 300 and 700 lbs were obtained from a meat abattoir. Aortic valves were carefully explanted to preserve the annulus, leaflets, left and right coronary arteries, and the ascending aorta. The distal left ventricular

outflow tract was mounted asymmetrically to a porcine-sized elastomeric sewing ring on a 3D-printed conduit mount using a running 4–0 polypropylene suture, such that the non-right commissure and the non-left commissure were both shifted slightly towards the left-right commissure, resulting in a 140–160° angle for the non-coronary cusp (Figure 1A). Next, the left and right coronary cusps were “fused” together using a running CV-6 polytetrafluoroethylene (PTFE) suture (Gore-Tex® Suture, WL Gore & Associates Inc., Flagstaff, Arizona). To fully imitate the geometry of a human BAV with left-right cusp fusion, the height of the left-right commissure from the level of the aortic annulus was measured. This commissure was then carefully detached. A small portion of the two cusps supported by this commissure was also carefully detached from the annulus to allow for commissural manipulation. The commissure was then re-implanted 10 mm below the native height. (Figure 1B) The base of the detached aortic cusps was re-anastomosed to the aortic annulus using a running 6–0 polypropylene suture. Lastly, to reduce the ascending aorta diameter to fit the porcine-sized outflow mount and to translate the aortic wall tissue to reflect asymmetric commissure positioning, a wedge of ascending aortic wall tissue was resected above the left-right commissure (Figure 1C). The residual aortic wall tissues were re-anastomosed together using a running 4–0 polypropylene suture (Figure 1D). The valves were subsequently repaired using free margin shortening technique using CV-6 PTFE sutures. The step-by-step demonstration of the model generation is shown in Supplementary Figure 1.

To assess the BAV model in comparison to normal valves, 3 porcine control aortic valves were explanted from hearts obtained from a meat abattoir and mounted onto the conduit in a symmetrical fashion without any additional modification.

### Left Heart Simulator

To quantitatively analyze the efficacy of our model as well as examine the repair, we used our custom left heart simulator that has been previously described in detail (Supplementary Figure 2)<sup>17–19</sup>. The simulator features a programmable pulsatile linear piston pump (ViVitro Superpump, ViVitro Labs, Victoria, BC, Canada) and a viscoelastic impedance adapter (ViVitro) that generates a physiologic ventricular waveform. The viscoelastic impedance adaptor is comprised of two compliance chambers and a fixed resistance element (200 dyne·s/cm<sup>5</sup>). The circuit additionally contains a separate aortic compliance chamber (maximum air volume of 940 ml) and an adjustable peripheral resistance. With the pump stroke volume set to 110 mL, the compliance and peripheral resistance were titrated to generate physiologic systolic and diastolic arterial pressures. We utilized pressure transducers (Utah Medical Products Inc., Midvale, Utah) and electromagnetic flow probes (Carolina Medical Electronics, East Bend, North Carolina) to record aortic, left ventricular, and left atrial pressure and flow throughout a complete cardiac cycle. The simulator was calibrated using a mechanical aortic valve to ensure the pump was set to generate an effective stroke volume of 70 mL at 70 beats per minute. The hemodynamics data was collected and averaged across ten cycles at each stage of testing. To evaluate leaflet morphology and motion, high-speed videography was obtained with an en face view at 1057 frames per second with 1280×1024 resolution (Chronos 1.4, Kron Technologies, Burnaby, British Columbia, Canada).

## Echocardiography Measurements

A Phillips iE33 system with an X7–2T transesophageal and S5–1 transthoracic probe (Koninklijke Philips NV, Amsterdam, The Netherlands) was used to obtain echocardiographic data with short- and long-axis views and color flow mappings. Continuous-wave doppler was also obtained. Data analysis was performed using the iE33 on-board software and a Siemens Syngo Dynamics workstation (Siemens Medical Solutions USA, Inc., Ann Arbor, MI). Images and calculations were reviewed by a pediatric cardiologist.

## Statistical Analysis

Based on our previous studies, to detect a 15% difference in mean regurgitant fraction with an estimated variance of 16, power of 80%, and confidence interval of 95%, a sample size of 2 is required. To ensure adequate power for the study, a sample size of 3 was chosen. Variance of each group was assessed using the F-test. A two-sampled paired t-test was performed to compare baseline BAV to post-repair BAV, while independent t-tests were performed to compare control to baseline BAV and to post-repair BAV. Continuous variables are reported as mean  $\pm$  standard deviation. Statistical significance was defined at  $p < 0.05$  for all tests. Approval by the Institutional Animal Care and Use Committee was not indicated for this study as the hearts were purchased from a meat abattoir.

## RESULTS

### Baseline BAV Model

Our novel BAV model closely simulated the human BAV pathology with left-right cusp fusion and prolapse, resulting in AR. The non-coronary cusp spanned an average angle of  $149 \pm 9^\circ$ . Figure 2A presents a representative example of our BAV disease model during diastole with prolapse of the fused cusp and a regurgitant fraction of 32.5%. Our BAV model consistently produced left-right fused cusp prolapse with an average regurgitant fraction of  $28.6 \pm 3.4\%$ , significantly higher than that from the controls ( $9.3 \pm 2.3\%$ ,  $p = .0002$ ). Mean aortic flow tracings and pressure tracings of the BAV model are shown in Figure 3A and 3B, with shaded regions representing standard deviation. AR was confirmed in our model from the mean aortic flow tracings, as evidenced by the flow reversal observed in diastole. Mean arterial pressure measured for our BAV model was  $81.1 \pm 1.2$  mmHg with a diastolic pressure of  $61.7 \pm 2.1$  mmHg and a systolic pressure of  $104.2 \pm 0.9$  mmHg. Hemodynamics data are shown in Table 1.

The high-speed videography demonstrated restricted leaflet motion of the fused cusp during systole and prolapse of the fused cusp during diastole (Supplemental Material Video 1, Video 2). Echocardiographic images similarly showed moderate AR with eccentric, posteriorly directed jets in our BAV model (Figure 4A, Supplemental Material Video 3). The aortic valve leaflets were restricted and domed in systole.

### BAV Model After Repair

Free margin shortening was the primary technique utilized to repair the prolapsed fused cusp. Figure 2B presents a representative example of the same BAV disease

model illustrated in Figure 2A after repair during diastole with a regurgitant fraction of 16.7%. After repair, the regurgitant fraction was significantly reduced ( $28.6\pm 3.4\%$  versus  $14.5\pm 4.4\%$ ,  $p=.037$ ). The regurgitant fractions for the repaired BAVs were similar to those for the controls ( $14.5\pm 4.4\%$  versus  $9.3\pm 2.3\%$ ,  $p=.17$ ). Mean aortic flow tracings of repaired BAV models demonstrated no flow reversal in diastole (Figure 3A). Aortic pressure tracings (Figure 3B) also demonstrated increased pressures throughout the cardiac cycle compared to the baseline measurements with a mean arterial pressure of  $94.3\pm 1.6$  versus  $81.1\pm 1.2$  mmHg ( $p=0.009$ ), diastolic pressure of  $76.3\pm 3.6$  versus  $61.7\pm 2.1$  mmHg ( $p=0.03$ ), and systolic pressure of  $119.1\pm 1.1$  versus  $104.2\pm 0.9$  mmHg ( $p=0.003$ ), respectively. Hemodynamics data post-repair are shown in Table 1.

The high-speed videography of the repaired valves demonstrated restricted leaflet motion of the fused cusp during systole but adequate coaptation of the cusps during diastole (Supplemental Material Video 4, Video 5). Echocardiographic images similarly showed no significant AR, although aortic leaflets were still restricted and doming in systole (Figure 4B, Supplemental Material Video 6). Each of the following metrics were similar when comparing repaired BAV versus baseline BAV, control versus baseline BAV, and control versus repaired BAV: peak aortic jet velocity ( $325\pm 58.2$  versus  $293.3\pm 18.3$  cm/s,  $p=0.29$ ;  $363.7\pm 52.5$  versus  $293.3\pm 18.3$  cm/s,  $p=.09$ ;  $363.7\pm 52.5$  versus  $325\pm 58.2$  cm/s,  $p=.44$ ), peak instantaneous systolic gradient ( $43.3\pm 15.4$  versus  $34.3\pm 4.2$  mmHg,  $p=0.30$ ;  $54.0\pm 15.9$  versus  $34.3\pm 4.2$  mmHg,  $p=.11$ ;  $54.0\pm 15.9$  versus  $43.3\pm 15.4$  mmHg,  $p=.45$ ) and mean gradient ( $9.3\pm 2.5$  versus  $11.0\pm 1.0$  mmHg,  $p=0.34$ ;  $9.7\pm 3.8$  versus  $11.0\pm 1.0$  mmHg,  $p=.59$ ;  $9.7\pm 3.8$  versus  $9.3\pm 2.5$  mmHg,  $p=.91$ ).

## DISCUSSION

In this study, we successfully developed a clinically relevant *ex vivo* BAV model with left-right cusp fusion and AR to reproduce the most prevalent phenotype of human BAV with prolapse of the fused cusp (Figure 5). This model was achieved by mounting the commissures asymmetrically, lowering the commissure between the fused cusps, relieving the rotational tension in the ascending aorta, and fusing the left and right coronary cusps. AR was confirmed through hemodynamics data and echocardiographic measurements. This model was also repairable, as evidenced by hemodynamics and echocardiographic data, demonstrating its potential in the evaluation of BAV surgical repair techniques.

Traditionally, porcine aortic valves are selected as a human analog due to the similarities in size and anatomy to human aortic valves<sup>20,21</sup>. However, porcine aortic valves were found to be unsuitable for this study due to the lack of redundant tissue that is needed to successfully manipulate the cusp tissue. Small bovine aortic valves, on the other hand, provide additional tissue that mimic the chronic adaptation of aortic cusps in the setting of AR, allowing us to generate adequate cusp prolapse<sup>22</sup>. Additionally, porcine aortic cusps are much thinner compared to those of humans, whereas bovine aortic cusps are similar in thickness compared to those of humans<sup>23,24</sup>. The appropriate aortic cusp thickness in our BAV model is crucial in the valve's tolerability of tissue manipulation and repair.

Our model is unique in that it very closely mimics the most common human BAV valve morphology associated with AR without echocardiographic evidence of aortic stenosis compared to normal control valves. A contemporary study reported an *ex vivo* porcine model of BAV that was generated by bicuspidization of the left and right coronary cusps and the left and non-coronary cusps using running sutures<sup>25</sup>. However, this model did not fully capture the detailed differences between a BAV compared to a trileaflet aortic valve besides fused cusps. Previous studies have published different BAV classifications<sup>3,5</sup>. The Sievers classification is one of the most commonly used BAV classifications<sup>3</sup>. Type I BAV with left-right coronary cusp fusion was noted to be the most prevalent morphology<sup>3</sup>. de Kerchove et al. recently demonstrated variabilities in repairable BAV phenotypes and illustrated that besides the six Sievers BAV morphologies, the BAV phenotypes follow a continuous spectrum that extends from symmetrical to very asymmetrical BAV with variations in commissural orientation, length of fusion and non-functional commissure height<sup>5</sup>. Our novel BAV model recapitulates the most common phenotype, Sievers type I BAV, and also mimics the type B asymmetric BAV phenotype as described by de Kerchove et al. with similar commissural orientation and height difference between the non-functional commissure and the other commissures<sup>5</sup>. It is also worth mentioning that the type B asymmetric BAV described by de Kerchove et al. has the highest likelihood to present with moderate to severe AR, likely due to unequal cusp surface area and uneven commissural height leading to inadequate coaptation area<sup>3,5</sup>. The capability to generate AR with our novel BAV model is crucial to the future application of our disease model for the evaluation of surgical repair techniques for BAV. We have also observed varied degrees of AR generated using different commissural locations in terms of suspension height and the angle of the non-coronary cusp, suggesting the importance of commissural position in maintaining leaflet functionality. Moreover, the AR associated with our BAV model was validated by echocardiography, the most clinically relevant modality. This can further enable the easy translation of our findings to clinical practice.

Aortic valve repair techniques have evolved in the modern era and have included the development of a systematic approach to BAV repair<sup>10,26,27</sup>. Long-term durability of BAV repair, however, was found to be likely influenced by leaflet geometry which can induce a varied level of aortic wall stress<sup>28-30</sup>. Some have advocated the conversion of the Sievers type I to a type 0 morphology in BAV repair using techniques such as raphe resection, annular detachment, enlargement, reinforcement, and translocation in order to achieve superior aortic wall stress levels<sup>31,32</sup>. However, it is important to note that the repair techniques utilized for different BAV morphology may vary significantly<sup>5</sup>. Utilization of a “standard” BAV repair technique without considering the leaflet morphology may result in increased stress in the repaired leaflet, resulting in early repair failure<sup>33,34</sup>. In this study, we demonstrated that by using free margin shortening, successful repair can be performed. Although a small residual regurgitant fraction was detected after repair, this is comparable to the regurgitant fraction of normal control valves and reflects the backward aortic flow during early diastole. Our control regurgitant fraction is consistent with results from previous studies using phase contrast velocity mapping<sup>35</sup>. Additionally, there was no statistically significant increase in peak velocity, peak gradient, or mean gradient across the valve after repair compared to normal control valves. This study is a precursor of comprehensive repair

technique evaluation using an *ex vivo* model. Further trials are needed to explore the clinical impact of various repair techniques for different BAV phenotype to provide guidance in surgical management.

Patient-specific computer simulation has gained recent interest and has shown potential in assessing feasibility of intervention and understanding valvular pathologies<sup>36</sup>. While these tools have proven to be valuable in obtaining insights into valvular biomechanics, there are key computational and methodological obstacles to obtaining a clinically relevant model that would allow for accurate patient-specific simulation of a given repair technique<sup>36</sup>. In contrast, our model provides direct measurement of hemodynamics data and allows for visualization of valvular function in a pressurized environment throughout the cardiac cycle, which is impossible to achieve in human. Additionally, our model system can also provide direct assessment of all repair techniques in a randomized fashion, which would be unethical and impractical to perform in human subjects.

One limitation of this model is the inability to fully simulate the degenerative state of BAV that commonly occurs in patients with BAV needing repair or replacement. Additionally, our model only recapitulated one BAV phenotype, whereas a spectrum of BAV morphology exists. Further development of other BAV phenotypes is warranted to fully represent the BAV disease state. This will also allow us to compare hemodynamic differences among the spectrum of BAV morphology. Although our model could generate moderate AR, severe AR has not been successfully produced. We suspect that the redundant tissue innate in cow aortic valve prohibits severe cusp mal-alignment. Lastly, though this study only evaluated the free margin shortening repair technique to validate model reparability, a more comprehensive evaluation of all BAV repair techniques can be investigated to evaluate for repair efficacy and the associated hemodynamic impacts.

## Supplementary Material

Refer to Web version on PubMed Central for supplementary material.

## ACKNOWLEDGMENTS

This work was supported by the National Institutes of Health (NIH R01 HL089315-01, YJW), the Thoracic Surgery Foundation Resident Research Fellowship (YZ), the National Science Foundation Graduate Research Fellowship Program (DGE-1656518, AMI), and the American Heart Association (17POST33410497, MJP). We would also like to thank the generous donation by Kevin Taweel to support this research effort.

### Disclosure and Funding:

The authors have no conflicts of interest or financial relationships with industry to disclose. This work was supported by the National Institutes of Health (NIH R01 HL089315-01, YJW), the Thoracic Surgery Foundation Resident Research Fellowship (YZ), the National Science Foundation Graduate Research Fellowship Program (DGE-1656518, AMI), and the American Heart Association (17POST33410497, MJP). The content is solely the responsibility of the authors and does not necessarily represent the official views of the funders.

## Glossary of Abbreviations

<b>BAV</b>	Bicuspid aortic valve
<b>AR</b>	Aortic regurgitation

<b>PTFE</b>	Polytetrafluoroethylene
<b>RMS</b>	Root mean square
<b>SD</b>	Standard deviation

## REFERENCES

1. Zhu Y, Roselli EE, Idrees JJ, Wojnarski CM, Griffin B, Kalahasti V, et al. Outcomes After Operations for Unicuspid Aortic Valve With or Without Ascending Repair in Adults. *Ann Thorac Surg.* 2016;101:613–9. [PubMed: 26453423]
2. Siu SC, Silversides CK. Bicuspid Aortic Valve Disease. *J Am Coll Cardiol.* 2010;55:2789–800. [PubMed: 20579534]
3. Ridley CH, Vallabhajosyula P, Bavaria JE, Patel PA, Gutsche JT, Shah R, et al. The Sievers Classification of the Bicuspid Aortic Valve for the Perioperative Echocardiographer: The Importance of Valve Phenotype for Aortic Valve Repair in the Era of the Functional Aortic Annulus. *J Cardiothorac Vasc Anesth.* 2016;30:1142–51. [PubMed: 27241768]
4. Boodhwani M, De Kerchove L, Glineur D, Rubay J, Vanoverschelde JL, Noirhomme P, et al. Repair of regurgitant bicuspid aortic valves: A systematic approach. *J Thorac Cardiovasc Surg.* 2010;140:276–84. [PubMed: 20488466]
5. de Kerchove L, Mastrobuoni S, Froede L, Tamer S, Boodhwani M, van Dyck M, et al. Variability of repairable bicuspid aortic valve phenotypes: towards an anatomical and repair-oriented classification. *Eur J Cardiothorac Surg.* 2019;56:351–9.
6. de Kerchove L, Glineur D, Poncelet A, Boodhwani M, Rubay J, Dhoore W, et al. Repair of aortic leaflet prolapse: a ten-year experience. *Eur J Cardio-thoracic Surg.* 2008;34:785–91.
7. Fraser CD, Wang N, Mee RBB, Lytle BW, McCarthy PM, Sapp SK, et al. Repair of insufficient bicuspid aortic valves. *Ann Thorac Surg.* 1994;58:386–90. [PubMed: 8067836]
8. Casselman FP, Gillinov AM, Akhrass R, Kasirajan V, Blackstone EH, Cosgrove DM. Intermediate-term durability of bicuspid aortic valve repair for prolapsing leaflet. *Eur J Cardiothorac Surg.* 1999;15:302–8. [PubMed: 10333027]
9. Augoustides J, Szeto WY, Bavaria JE. Advances in aortic valve repair: focus on functional approach, clinical outcomes, and central role of echocardiography. *J Cardiothorac Vasc Anesth.* 2010;24:1016–20. [PubMed: 20952208]
10. Vohra H, Whistance RN, De Kerchove L, Punjabi P, El Khoury G. Valve-preserving surgery on the bicuspid aortic valve. *Eur J Cardiothorac Surg.* 2013;43:888–98. [PubMed: 23293321]
11. De Kerchove L, Boodhwani M, Glineur D, Vandyck M, Vanoverschelde JL, Noirhomme P, et al. Valve sparing-root replacement with the reimplantation technique to increase the durability of bicuspid aortic valve repair. *J Thorac Cardiovasc Surg.* 2011;142:1430–8. [PubMed: 21955470]
12. Schneider U, Schmied W, Aicher D, Giebels C, Winter L, Schäfers HJ. Sinus Plication to Improve Valve Configuration in Bicuspid Aortic Valve Repair—Early Results. *Ann Thorac Surg.* 2017;103:580–5. [PubMed: 27623278]
13. Paulsen MJ, Imbrie-Moore AM, Wang H, Bae JH, Hironaka CE, Farry JM, et al. Mitral chordae tendineae force profile characterization using a posterior ventricular anchoring neochordal repair model for mitral regurgitation in a three-dimensional-printed ex vivo left heart simulator. *Eur J Cardiothorac Surg.* 2020;57:535–44. [PubMed: 31638697]
14. Imbrie-Moore AM, Paullin CC, Paulsen MJ, Grady F, Wang H, Hironaka CE, et al. A novel 3D-Printed preferential posterior mitral annular dilation device delineates regurgitation onset threshold in an ex vivo heart simulator. *Med Eng Phys.* 2020;77:10–8. [PubMed: 32008935]
15. Imbrie-Moore AM, Paulsen MJ, Zhu Y, Wang H, Lucian HJ, Farry JM, et al. A novel cross-species model of Barlow's disease to biomechanically analyze repair techniques in an ex vivo left heart simulator. *J Thorac Cardiovasc Surg.* 2020. doi:10.1016/j.jtcvs.2020.01.086
16. Siefert AW, Rabbah JPM, Pierce EL, Kunzelman KS, Yoganathan AP. Quantitative Evaluation of Annuloplasty on Mitral Valve Chordae Tendineae Forces to Supplement Surgical Planning Model Development. *Cardiovasc Eng Technol.* 2014;5:35–43. [PubMed: 24634699]



17. Imbrie-Moore AM, Paulsen MJ, Thakore AD, Wang H, Hironaka CE, Lucian HJ, et al. Ex Vivo Biomechanical Study of Apical Versus Papillary Neochord Anchoring for Mitral Regurgitation. *Ann Thorac Surg.* 2019;108:90–7. [PubMed: 30836099]
18. Paulsen MJ, Kasinpila P, Imbrie-Moore AM, Wang H, Hironaka CE, Koyano TK, et al. Modeling conduit choice for valve-sparing aortic root replacement on biomechanics with a 3-dimensional-printed heart simulator. *J Thorac Cardiovasc Surg.* 2019;158:392–403. [PubMed: 30745047]
19. Zhu Y, Imbrie-Moore AM, Paulsen MJ, Priromprintr B, Park MH, Wang H, et al. A Novel Aortic Regurgitation Model from Cusp Prolapse with Hemodynamic Validation Using an Ex Vivo Left Heart Simulator. *J Cardiovasc Transl Res.* 2020. doi: 10.1007/s12265-020-10038-z.
20. Benhassen LL, Ropcke DM, Sharghbin M, Lading T, Skov JK, Tjørnild MJ, et al. Comparison of Dacron ring and suture annuloplasty for aortic valve repair—a porcine study. *Ann Cardiothorac Surg.* 2019;8:342–50. [PubMed: 31240178]
21. Wang C, Lachat M, Regar E, von Segesser LK, Maisano F, Ferrari E. Suitability of the porcine aortic model for transcatheter aortic root repair. *Interact Cardiovasc Thorac Surg.* 2018;26:1002–8. [PubMed: 29415164]
22. Kim DH, Handschumacher MD, Levine RA, Levine RA, Sun BJ, Jang JY, et al. Aortic Valve Adaptation to Aortic Root Dilatation Insights into the Mechanism of Functional Aortic Regurgitation from 3-Dimensional Cardiac Computed Tomography. *Circ Cardiovasc Imaging.* 2014;7:828–35. [PubMed: 25051951]
23. Li J, Luo XY, Kuang ZB. A Nonlinear Anisotropic Model for Porcine Aortic Heart Valves. *J Biomech.* 2001;34:1279–89. [PubMed: 11522307]
24. Sahasakul Y, Edwards WD, Naessens JM, Tajik AJ. Age-related changes in aortic and mitral valve thickness: Implications for two-dimensional echocardiography based on an autopsy study of 200 normal human hearts. *Am J Cardiol.* 1988;62:424–30. [PubMed: 3414519]
25. Juraszek A, Dziodzio T, Stoiber M, Fechtig D, Gschlad V, Aigner P, et al. The influence of bicuspid aortic valves on the dynamic pressure distribution in the ascending aorta: a porcine ex vivo model. *Eur J Cardiothorac Surg.* 2014;46:349–55. [PubMed: 24644312]
26. Prodromo J, D’Ancona G, Amaducci A, Pilato M. Aortic valve repair for aortic insufficiency: A review. *J Cardiothorac Vasc Anesth.* 2012;26:923–32. [PubMed: 22703946]
27. Komiya T. Aortic valve repair update. *Gen Thorac Cardiovasc Surg.* 2015;63:309–19. [PubMed: 25652725]
28. Jermihov PN, Jia L, Sacks MS, Gorman RC, Gorman JH, Chandran KB. Effect of Geometry on the Leaflet Stresses in Simulated Models of Congenital Bicuspid Aortic Valves. *Cardiovasc Eng Technol.* 2011;2:48–56. [PubMed: 21980326]
29. Mahadevia R, Barker AJ, Schnell S, Entezari P, Kansal P, Fedak PW, et al. Bicuspid aortic cusp fusion morphology alters aortic three-dimensional outflow patterns, wall shear stress, and expression of aortopathy. *Circulation.* 2014;129:673–82. [PubMed: 24345403]
30. Guzzardi D, Barker AJ, van Ooij P, Malaisrie SC, Puthumana JJ, Belke DD, et al. Valve-related hemodynamics mediate human bicuspid aortopathy: insights from wall shear stress mapping. *J Am Coll Cardiol.* 2015;66:892–900. [PubMed: 26293758]
31. Stephens E, Hope TA, Kari FA, Kvitting JP, Liang DH, Herfkens RJ, et al. Greater asymmetric wall shear stress in Sievers’ type 1/LR compared with 0/LAT bicuspid aortic valves after valve-sparing aortic root replacement. *J Thorac Cardiovasc Surg.* 2015;150:59–68. [PubMed: 25956338]
32. Gleason TG. Bicuspid aortic valve repair by complete conversion from “raphe’d”(type 1) to “symmetric”(type 0) morphology. *J Thorac Cardiovasc Surg.* 2014;148:2862–8. [PubMed: 24930615]
33. Aicher D, Kunihara T, Abou Issa O, Brittner B, Gräber S, Schäfers HJ. Valve configuration determines long-term results after repair of the bicuspid aortic valve. *Circulation.* 2011;123:178–85. [PubMed: 21200006]
34. Schneider U, Feldner SK, Hofmann C, Schöpe J, Wagenpfeil S, Giebels C, et al. Two decades of experience with root remodeling and valve repair for bicuspid aortic valves. *J Thorac Cardiovasc Surg.* 2017;153:S65–S71. [PubMed: 28168982]
35. Gulsin GS, Singh A, McCann GP. Cardiovascular magnetic resonance in the evaluation of heart valve disease. *BMC Med Imaging.* 2017;17:67. [PubMed: 29284450]

36. Votta E, Le TB, Stevanella M, Fusini L, Caiani EG, Redaelli A, et al. Toward Patient-Specific Simulations of Cardiac Valves: State-Of-The-Art and Future Directions. *J Biomech.* 2013;46:217–28. [PubMed: 23174421]

Author Manuscript

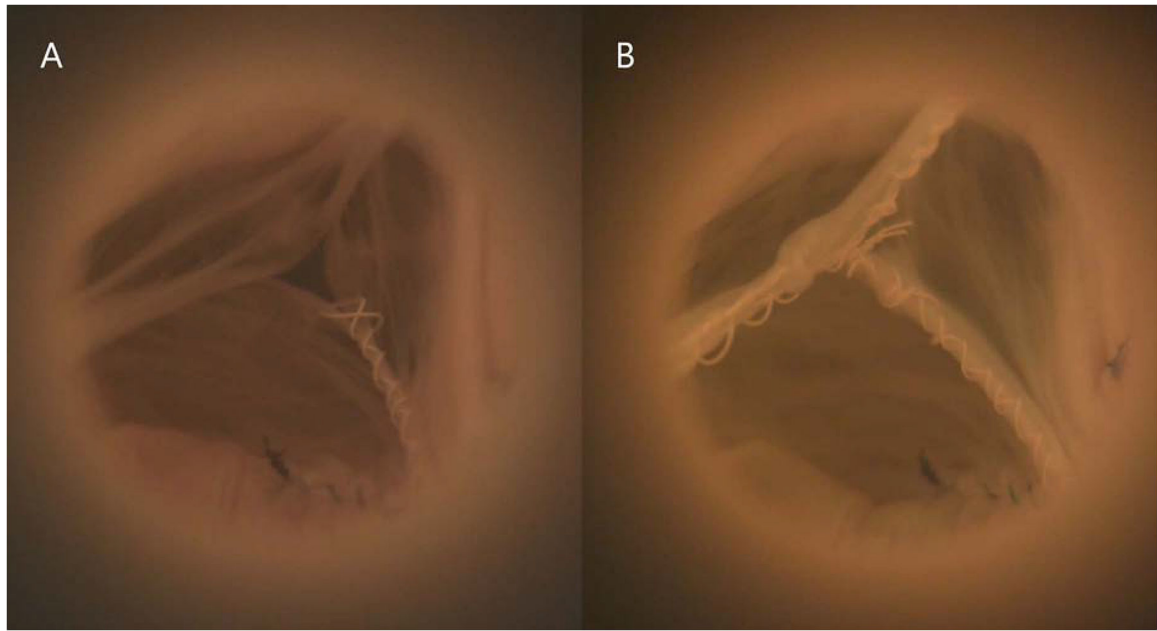
Author Manuscript

Author Manuscript

Author Manuscript

**PERSPECTIVE STATEMENT**

We designed a clinically relevant, cross-species *ex vivo* bicuspid aortic valve model with left-right cusp fusion. This model closely mimics the most prevalent human bicuspid aortic valve phenotype with prolapse of the fused cusp. This model was also repairable, demonstrating its potential in the evaluation of bicuspid aortic valve hemodynamics and surgical repair techniques.

**Figure 1:**

(A) En face illustration of the first steps of the bicuspid aortic valve (BAV) model design. The non-right commissure and the non-left commissure were each shifted towards the left-right commissure, resulting in a 140–160° angle for the non-coronary cusp. The left and right coronary cusps were “fused” together with a running suture. (B) A side view illustrating that the left-right commissure was carefully detached and re-implanted 10 mm below the native height. (C) A wedge of ascending aortic wall tissue was resected above the left-right commissure to translate the aortic wall tissue to reflect asymmetric commissure positioning. (D) The residual aortic wall tissue was re-anastomosed together using a running suture.

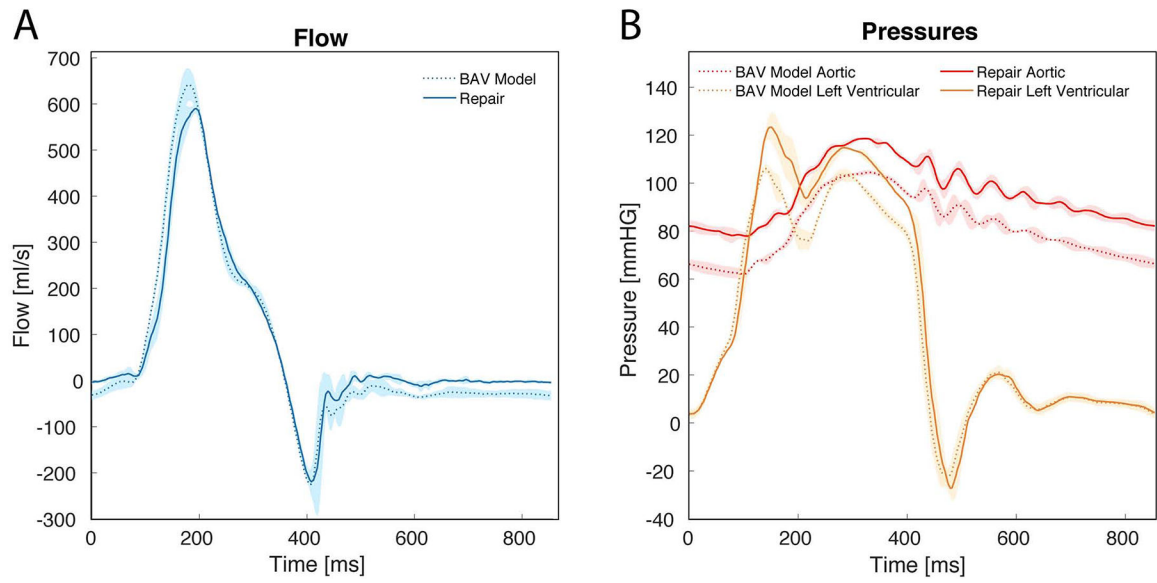


**Figure 2:**

(A) Baseline bicuspid aortic valve (BAV) model mounted in a left heart simulator, pictured in diastole. Note the prolapsed fused cusp. (B) The same BAV model in diastole after repair using free margin shortening.

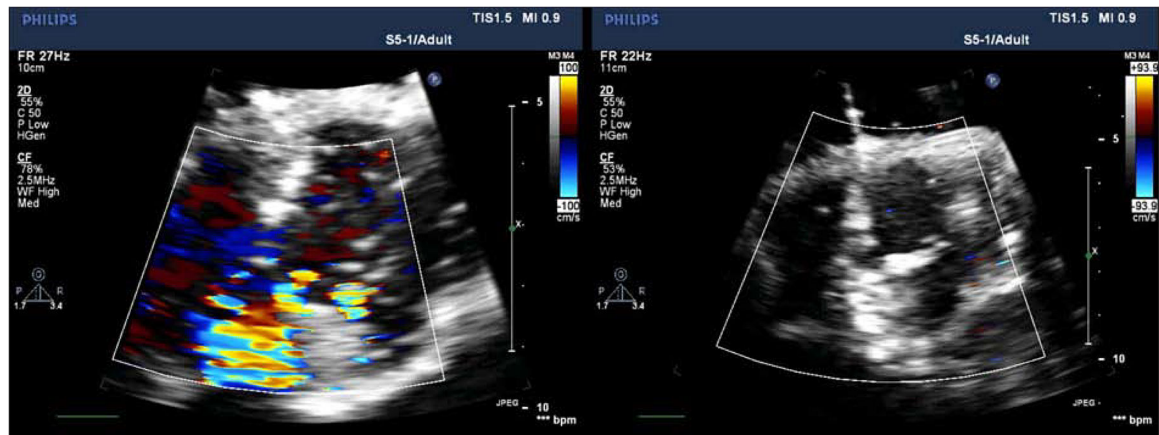


**Figure 3:**

(A) Mean aortic flow confirmed the generation of aortic regurgitation in our bicuspid aortic valve (BAV) model at baseline as evidenced by the flow reversal observed in diastole. After repair, the regurgitant fraction was significantly reduced ( $28.6 \pm 3.4\%$  versus  $14.5 \pm 4.4\%$ ,  $p = .014$ ). (B) Aortic pressure tracings demonstrated significantly lower pressures throughout the cardiac cycle for the BAV model at baseline compared to after repair: mean arterial pressure ( $81.1 \pm 1.2$  versus  $94.3 \pm 1.6$  mmHg,  $p < 0.001$ ), diastolic pressure ( $61.7 \pm 2.1$  versus  $76.3 \pm 3.6$  mmHg,  $p = 0.007$ ), and systolic pressure ( $104.2 \pm 0.9$  versus  $119.1 \pm 1.1$  mmHg,  $p < 0.001$ ). Shaded regions represent standard deviation.

**Novel Bicuspid Aortic Valve Model with Aortic Regurgitation for Hemodynamics Analysis Using an Ex Vivo Simulator**

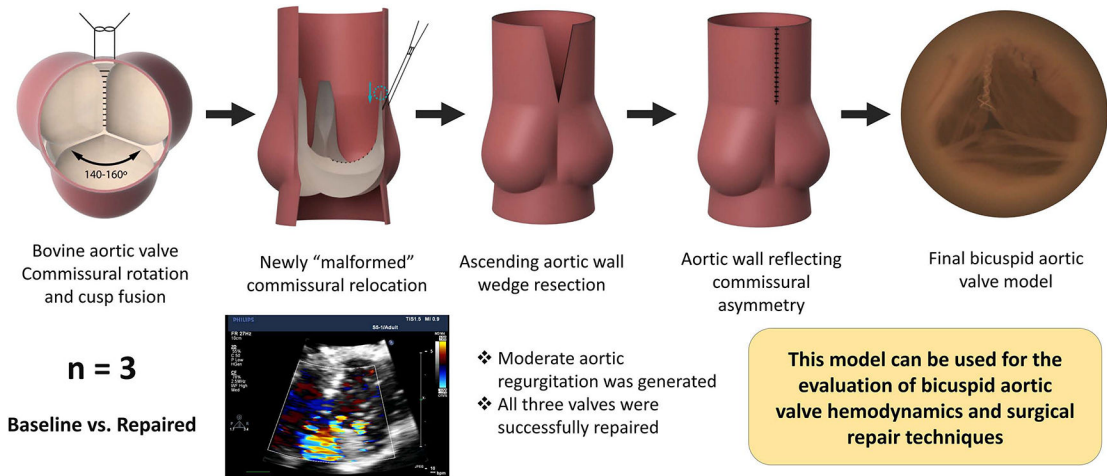


**Figure 4:** Echocardiography color flow mapping images in diastole reflecting (A) moderate aortic regurgitation (AR) with an eccentric jet in a representative example of our bicuspid aortic valve (BAV) model at baseline, and (B) significantly reduced AR after repair of the same BAV model.

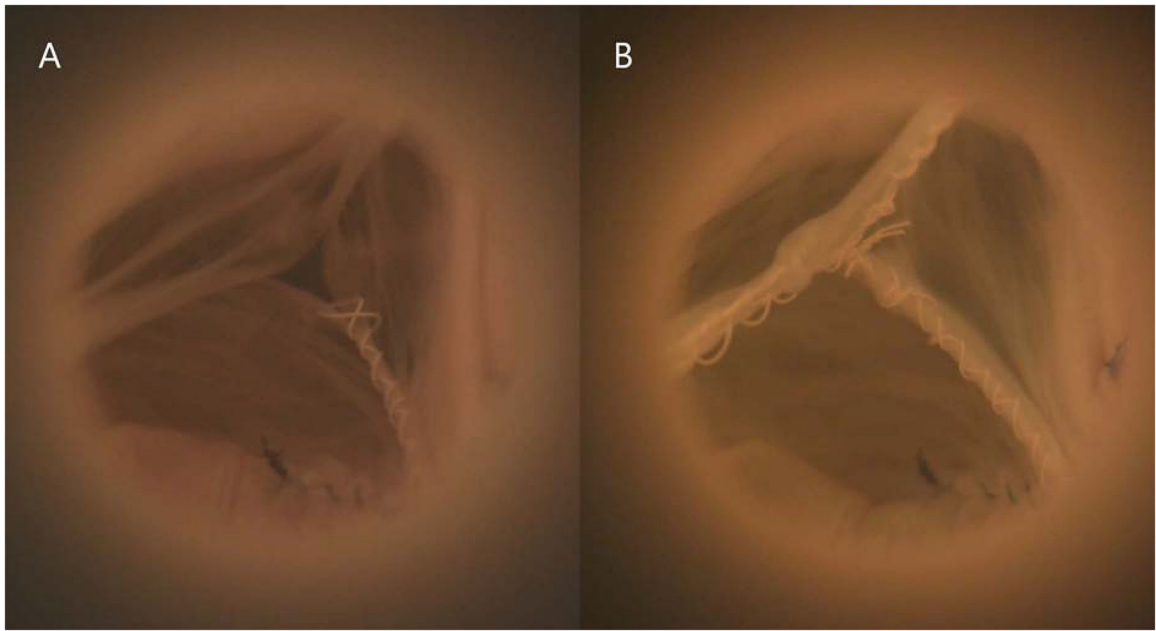
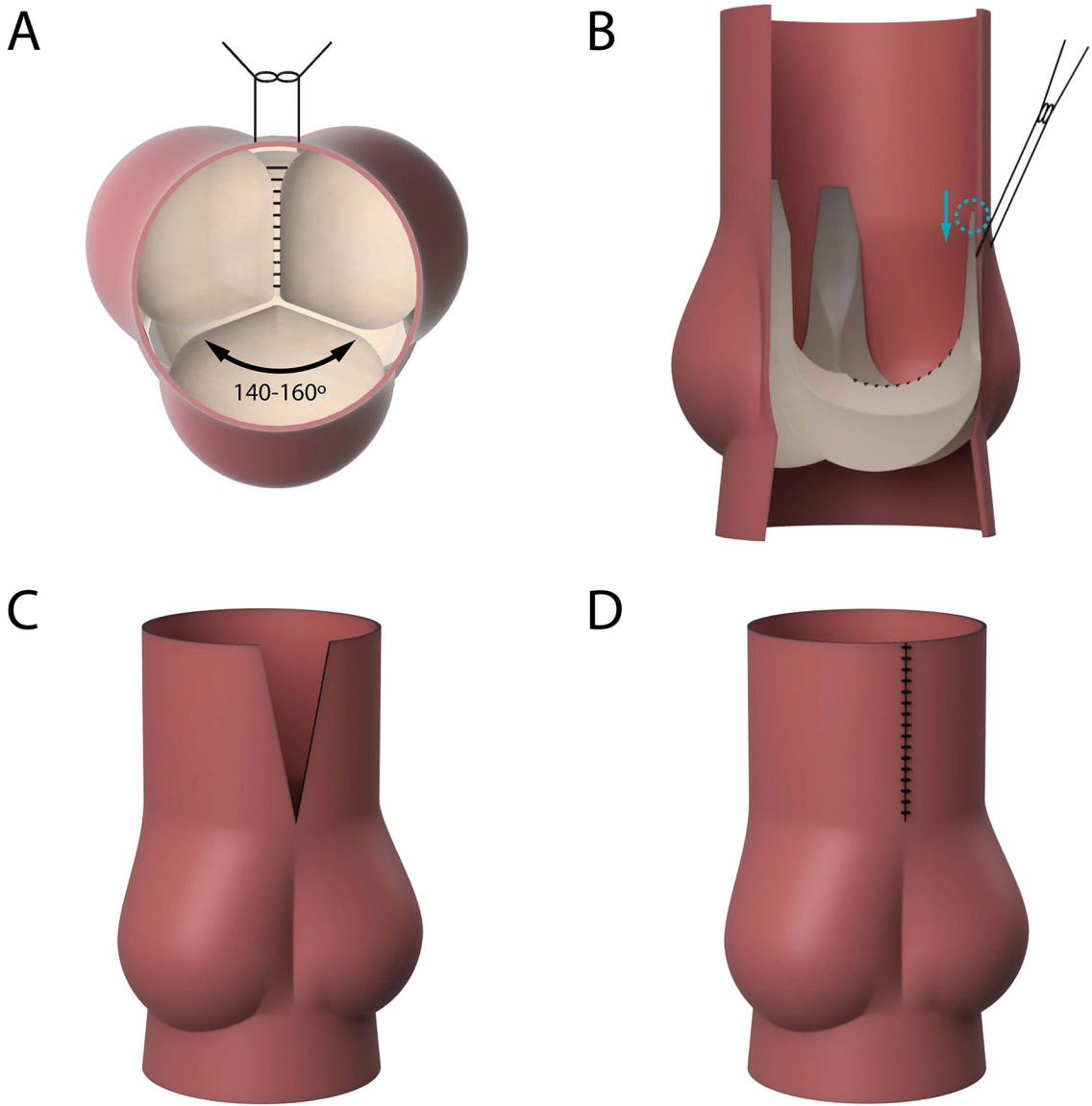


**Figure 5:**  
Novel bicuspid aortic valve model successfully created with associated aortic regurgitation for ex vivo hemodynamics analysis.





**CENTRAL PICTURE LEGEND.**

Novel bicuspid aortic valve model with prolapse of the fused cusp before and after repair.

Table 1 –

Hemodynamic Parameters

	BAV Baseline n=3 Mean±SD	BAV Repaired n=3 Mean±SD	Control n=3 Mean±SD	BAV Baseline versus BAV repaired P value	BAV Baseline versus Control P value	BAV Repaired versus Control P value
Heart rate (bpm)	70.0±0.0	70.0±0.0	70.0±0.0	1.000	1.000	1.000
Mean arterial pressure (mmHg)	81.1±1.2	95.4±1.6	98.5±0.9	<b>0.009</b>	< <b>0.001</b>	0.061
Systolic pressure (mmHg)	104.2±0.9	119.1±1.1	119.7±2.1	<b>0.003</b>	<b>0.002</b>	0.694
Diastolic pressure (mmHg)	61.7±2.1	76.3±3.6	80.9±0.2	<b>0.037</b>	<b>0.004</b>	0.159
Cardiac output (liters/min)	4.2±0.2	4.6±0.4	4.9±0.3	0.062	<b>0.017</b>	0.288
Effective stroke volume (ml)	59.7±2.7	66.0±5.2	70.6±3.7	0.062	<b>0.017</b>	0.288
Pump stroke volume (ml)	109.8±0.1	109.9±0.2	108.0±3.1	0.46	0.424	0.394
Aortic forward flow time (s)	0.3±0.0	0.3±0.0	0.3±0.0	0.73	0.612	0.654
Aortic forward volume (ml)	83.6±1.8	77.2±3.3	77.8±3.0	0.11	0.060	0.803
Aortic valve RMS forward flow rate (ml/s)	426.1±18.0	429.4±20.9	399.5±20.8	0.78	0.170	0.154
Effective orifice area (cm <sup>2</sup> )	2.6±0.6	2.2±0.6	2.3±0.8	0.30	0.588	0.861
Aortic regurgitant fraction (%)	28.6±3.4	14.5±4.4	9.3±2.3	<b>0.037</b>	<b>0.002</b>	0.172
Aortic leakage rate (ml/s)	-27.4±9.8	-1.7±3.8	-5.5±3.5	<b>0.026</b>	<b>0.048</b>	0.266
Aortic closing volume (ml)	-10.5±3.0	-10.3±3.2	-4.6±2.0	0.66	0.052	0.068
TransAortic forward energy loss (mJ)	81.7±10.5	87.6±39.5	137.3±105.6	0.81	0.458	0.510
TransAortic closing energy loss (mJ)	39.1±20.1	36.2±18.6	16.3±7.6	0.19	0.180	0.198
TransAortic leakage energy loss (mJ)	126.8±52.3	11.7±20.7	36.3±21.0	<b>0.039</b>	0.080	0.221
TransAortic total energy loss (mJ)	247.5±33.2	135.4±54.2	189.9±120.0	<b>0.024</b>	0.497	0.529

Abbreviations: BAV = bicuspid aortic valve; RMS = root mean square; SD = standard deviation.